Cordero-Cucart, MT.; Cerdán García, L.; Carbonell Olivares, A.; Katsarou, K.; Kalantidis, K.; Daros Arnau, JA. (2016). Dicer-like 4 is involved in restricting the systemic movement of Zucchini yellow mosaic virus in Nicotiana benthamiana. Molecular Plant-Microbe Interactions. 30(1):63-71. doi:10.1094/MPMI-11-16-0239-R.

# *Dicer-like 4* is involved in restricting the systemic movement of *Zucchini yellow mosaic virus* in *Nicotiana benthamiana*

**Teresa Cordero,[1] Lidia Cerdán,[1] Alberto Carbonell,[1] Konstantina Katsarou,[2] Kriton Kalantidis,[2] and José-Antonio Daròs[1]**

[1]Instituto de Biología Molecular y Celular de Plantas (Consejo Superior de Investigaciones Científicas-Universidad Politécnica de Valencia), 46022 Valencia, Spain; [2]Institute of Molecular Biology and Biotechnology, Foundation for Research and Technology; and Department of Biology, University of Crete, Heraklion, Crete, Greece

Corresponding author: J. A. Daròs

E-mail: jadaros@ibmcp.upv.es

***Zucchini yellow mosaic virus*** **(ZYMV) induces serious diseases in cucurbits. To create a tool to screen for resistance genes, we cloned a wild ZYMV isolate and inserted the visual marker *Rosea1* to obtain recombinant clone ZYMV-Ros1. While in some plant-virus combinations Rosea1 induces accumulation of anthocyanins in infected tissues, ZYMV-Ros1 infection of cucurbits did not lead to detectable anthocyanin accumulation. However, the recombinant virus did induce dark red pigmentation in infected tissues of the model plant *Nicotiana benthamiana*. In this species, ZYMV-Ros1 multiplied efficiently in local inoculated tissue but only a few progeny particles established infection foci in upper leaves. We used this system to analyze the roles of *Dicer-like* (*DCL*) genes, core components of plant antiviral RNA silencing pathways, in ZYMV infection. ZYMV-Ros1 local replication was not significantly affected in single *DCL*, nor in double *DCL2/4* and triple *DCL2/3/4* knock-down lines. ZYMV-Ros1 systemic accumulation was not affected in knock-down lines *DCL1*, *DCL2* and *DCL3*. However in *DCL4*, and also in *DCL2/4* and *DCL2/3/4* knock-down lines, ZYMV-Ros1 systemic accumulation dramatically increased, which highlights the key role of *DCL4* in restricting virus systemic movement. The effect of *DCL4* on ZYMV systemic movement was confirmed with a wild-type version of the virus.**

When plant viruses manage to enter an initial cell in their hosts, frequently with the help of a vector organism, they express and replicate their genomes to produce a progeny that first move cell to cell to reach the host vascular tissue, and then moves long-distance to distal areas. During this process, viruses hijack multiple elements, complexes and structures from host plants. They must also surpass all barriers and neutralize plant defensive responses. Viral and host components establish a complex interaction network that frequently leads to infection and disease response, but to resistance at other times. One of the main goals of plant virology is to understand this network in order to be able to modify the equilibrium to favor resistance.

Plants use RNA-mediated gene silencing pathways to fight invading viruses (Hamilton and Baulcombe, 1999). Plant Dicer-like (DCL) RNases recognize virus-specific double-stranded or highly-structured RNAs to produce 21-24 nucleotide (nt) small interfering RNA (siRNA) duplexes (Aliyari and Ding, 2009; Zhang et al., 2015). One of the strands is selectively loaded by an Argonaute (AGO) protein to guide the RNA-induced silencing complex (RISC) to target and repress sequence complementary viral RNAs (Carbonell and Carrington, 2015). The amount of viral double-stranded RNA that triggers the antiviral RNA silencing pathways in the host plant is amplified by RNA-dependent RNA (RDR) polymerase activities by using viral siRNAs as primers (Wang et al., 2010). In order to counteract this defensive response, evolution has shaped the proteins dedicated to suppress RNA silencing in virtually all plant viruses (Csorba et al., 2015).

*Zucchini yellow mosaic virus* (ZYMV) is a prominent pathogen of many plant species of the family *Cucurbitaceae*, which includes different important crops (Lecoq and Desbiez, 2012). It was first isolated in Italy in 1973 (Lisa et al., 1981), although it is currently present worldwide (Desbiez and Lecoq, 1997). ZYMV belongs to the genus *Potyvirus* in the family *Potyviridae*, and its genome consists of approximately 10,000 nt long single-stranded RNA molecules of plus polarity that encodes two versions of a large polyprotein (Wu et al., 2010). The genomic RNA of potyviruses (genus *Potyvirus*) is covalently attached at its 5' end to a viral protein genome-linked (VPg), contains a polyadenylated tail at its 3' end, and is encapsidated by approximately 2000 units of the viral coat protein (CP) in an elongated and flexuous virion (Revers and García, 2015). Potyviral proteins, which include the P1 protease, the helper component protease (HC-Pro), the P3 protein and P3N-PIPO, small hydrophobic polypeptide 6K1, the cylindrical inclusion (CI) protein, a second small hydrophobic polypeptide 6K2, the nuclear inclusion *a* (NIa) protein, which is further split in its two VPg and protease (NIaPro) domains, viral RDR polymerase or nuclear inclusion *b* (NIb) protein

and the CP (Fig. 1A), are produced from a regulated cascade of proteolytic processing through the activity of three viral proteases: P1, HC-Pro and NIaPro.

For purpose of obtaining a viral clone to facilitate screening for resistance in cucurbitaceous plants, we cloned a wild isolate of ZYMV and constructed a recombinant clone that expresses the snapdragon (*Antirrhinum majus* L.) *Rosea1* marker gene, which activates anthocyanins, a class of flavonoid pigments, biosynthesis and allows the visual tracking of viral infection in different plant species (Bedoya et al., 2012). Anthocyanin accumulation is cell-autonomous and only occurs in those cells infected by the marked virus in which Rosea1 is expressed. The amount of anthocyanins correlates with viral load (Bedoya et al., 2012). Unlike fluorescent protein markers, pigment accumulation in this system is clearly visible to the naked eye (Majer et al., 2013). We observed that this tool proved quite useless in zucchini (*Cucurbita pepo* L.) and other cucurbits, ZYMV natural hosts, given a negligible accumulation of colored anthocyanins in infected tissues. However in experimental host *Nicotiana benthamiana* Domin, efficient virus local multiplication in inoculated tissues, and an inefficient systemic movement to distal tissues, were observed for the recombinant clone. We reasoned that the *Rosea1*-marked ZYMV clone and *N. benthamiana* combination could represent an excellent experimental system to study the virus sequence determinant and the host factors involved in the long-distance movement of this virus. By means of this novel tool, we particularly aimed to analyze the differential contributions of the four *N. benthamiana DCL* genes, core components of the host RNA silencing pathways, in virus systemic movement in *N. benthamiana*. Our results show that while individual *DCL* genes barely contributed to inhibit virus multiplication in inoculated tissues, *DCL4* plays a major role in restricting ZYMV systemic movement in *N. benthamiana*.

## RESULTS

### A ZYMV infectious clone that includes the visual *Rosea1* marker suboptimally moves long-distance in *N. benthamiana*

The Rosea1 marker system has been successfully applied to several combinations of viruses and host plants (Bedoya et al., 2012). However, it cannot be considered as a universal system as it is based on the activity of an heterologous transcription factor on a host endogenous metabolic pathway. We wondered whether this system could be applied to ZYMV to track infection in cucurbitaceous plants. If this were the case, the system would be a most valuable tool to facilitate high-throughput screening for resistance in

cucurbit breeding programs. To this end, we cloned a wild ZYMV isolate from a zucchini plant (cultivar Scallop), grown in 2013 in Horta de Vera (Valencia, east Spain), which presented severe infection symptoms. Two internal cDNA fragments from the viral genome were amplified by reverse transcription (RT)-polymerase chain reaction (PCR), whereas the 5' and 3' terminal cDNAs were amplified by a rapid amplification of cDNA ends (RACE) strategy. The sequence information from all these cDNAs served to design a set of primers (see Supplementary Table S1) to amplify the whole genome of the Vera isolate of ZYMV in three cDNA fragments flanked by the recognition site of a type-IIS restriction enzyme. These fragments were finally assembled into a binary plasmid in which the full-length ZYMV cDNA was flanked by *Cauliflower mosaic virus* (CaMV) 35S promoter and a 50 nt-long poly(A) stretch followed by CaMV 35S terminator. This ZYMV cDNA was sequenced and the resulting full-length sequence was deposited in GenBank as the Vera isolate of ZYMV (GenBank accession number KX499498). A standard nucleotide BLAST search displayed the highest identity with a Taiwanese isolate of ZYMV (GenBank accession number AF127929.2) (Lin et al., 2001). An alignment analysis using ClustalW exhibited 94.6% nucleotide identity between both sequences with 517 nucleotide differences.

Next we inserted a cDNA that corresponded to the *A. majus Rosea1* coding region between ZYMV NIb and CP cistrons to construct the recombinant virus clone ZYMV-Ros1 (Fig. 1A). *Rosea1* cDNA was flanked by sequences that code for amino acids that complement both sides of the native NIb/CP proteolytic site to mediate the release of Rosea1 from the viral polyprotein (Fig. 1A and Supplementary Fig. S1). The *Agrobacterium tumefaciens* clones transformed with plasmids to express ZYMV (pGZYMV) or ZYMV-Ros1 (pGZYMV-Ros1), as well as the empty binary plasmid (pG35Z), were used to inoculate zucchini plants (cultivar MU-CU-16). All the plants agroinoculated with ZYMV or ZYMV-Ros1 became infected. The pictures taken on day 21 post-inoculation (dpi) show the severe symptoms induced by the Vera isolate of ZYMV (Fig. 1B and Supplementary Fig. S2). The plants infected by ZYMV-Ros1 showed milder symptoms (Fig. 1B and Supplementary Fig. S2). A Western blot analysis showed that accumulation of both viruses in upper non-inoculated leaves of zucchini plants was similar (Fig. 1C and D). Unfortunately, the infected tissues of these plants did not show the expected reddish pigmentation that Rosea1 induces in other species. Similar results were obtained with a different cucurbit species, melon (*Cucumis melo* L.) plants of the Piel de Sapo cultivar (Supplementary Fig. S3).

To confirm that recombinant clone ZYMV-Ros1 expressed a functional copy of Rosea1, we agroinoculated *N. benthamiana* plants using the same *A. tumefaciens* cultures.

ZYMV replicates with no symptoms in the inoculated leaves of *N. benthamiana* and, depending on the strain, moves systemically and induces latent infection (Desbiez and Lecoq, 1997). We previously showed that this species produces intense reddish pigmentation when infected with several viruses that express Rosea1, including other potyviruses like *Tobacco etch virus* (TEV) (Bedoya et al., 2012). Unlike the tissues agroinoculated with the empty vector or with ZYMV, tissues agroinoculated with ZYMV-Ros1 displayed intense dark red pigmentation at 7 dpi (Fig. 2A and Supplementary Fig. S4A). This result indicates that ZYMV-Ros1 expresses a functional Rosea1 transcription factor that efficiently induces accumulation of reddish anthocyanins in *N. benthamiana*. As expected, none of the *N. benthamiana* plants showed infection symptoms (Supplementary Fig. S4B). However, a prolonged observation of these plants revealed that, in those agroinoculated with ZYMV-Ros1, some pigmented foci constantly appeared to be scattered on the upper non-inoculated leaves (Fig. 2B). This result suggests that the Vera isolate of ZYMV is able to move long-distance in *N. benthamiana*, but inefficiently. It is noteworthy that we detected infection foci on the upper non-inoculated leaves due to the vivid pigmentation induced by the Rosea1 transcription factor. We realized that the combination of the ZYMV-Ros1 clone and *N. benthamiana* could represent a convenient experimental system to analyze elements involved in ZYMV systemic movement.

**Analysis of the contribution of the four host *DCL* genes to ZYMV systemic movement in *N. benthamiana***

With this experimental system at hand, we next aimed to study the effect of the four *N. benthamiana DCL* genes, which are core components of host RNA-mediated silencing pathways, on the systemic movement of ZYMV in this species. To this end, we used a set of *N. benthamiana* transgenic plants in which the different *DCL* genes were down-regulated by expressing specific hairpin constructs (Dadami et al., 2013; Katsarou et al., 2016). RT-quantitative PCR (RT-qPCR) and northern blot hybridization analyses of transgenic lines DCL1.13i, DCL2.11i, DCL3.10i and DCL4.9i showed a specific reduction in the *DCL1*, *DCL2*, *DCL3* and *DCL4* mRNAs levels, respectively. Apart from the plants knock-down in the single *DCL* genes, we also used line DCL2/4.5i, which expresses a hairpin to simultaneously down-regulate *DCL2* and *DCL4*, and line DCL3.10(x)2/4.5i, the heterozygous progeny that results from crossing DCL3.10i as a female and DCL2/4.5i as a male (Dadami et al., 2013; Katsarou et al., 2016).

We first questioned whether these genes had an effect on virus accumulation in inoculated tissue. For this purpose, we agroinoculated two leaves of three *N. benthamiana* plants that corresponded to the wild-type and the *DCL* knock-down lines DCL1.13i, DCL2.11i, DCL3.10i, DCL4.9i, DCL2/4.5i and DCL3.10(x)2/4.5i. The agroinoculated tissues were harvested at 6 dpi and proteins were extracted. ZYMV CP was analyzed by electrophoretic separation followed by Western blot using a specific anti-CP antibody (Fig. 3). Wild-type non-inoculated controls were added to the analysis. The quantification of the Western blot signals is summarized in Supplementary Table S2. Fig. 3 shows the three Western blots, as well as the graph of ZYMV CP accumulation in the agroinoculated tissue of the different *N. benthamiana* lines. According to the amount of CP, ZYMV-Ros1 accumulation in the inoculated tissues of the DCL1.13i, DCL2.11i, DCL4.9i and DCL2/4.5i lines was similar to that of the wild-type plants. ZYMV-Ros1 accumulation was lower in the DCL3.10i line (0.6-fold on average) and higher in the DCL3.10(x)2/4.5i line (1.75-fold on average) compared with the wild-type plants (Fig. 3B). However, none of the differences in ZYMV-Ros1 accumulation between wild-type and each of the *DCL* knock-down lines was statistically significant ($P < 0.05$ for all pair-wise Student's *t* test comparisons).

Next we analyzed the effect of the *DCL* down-regulation on ZYMV systemic movement in *N. benthamiana*. Sets of three plants that corresponded to the wild-type and the different knock-down lines were agroinoculated with ZYMV-Ros1 in three leaves. In the *N. benthamiana* lines DCL1.13i, DCL2.11i and DCL3.10i, we obtained the same outcome previously obtained in the wild-type plants. Very few infection foci were detected in the upper non-inoculated tissues. However in the *N. benthamiana* line DCL4.9i, and in lines DCL2/4.5i and DCL3.10(x)2/4.5i, ZYMV-Ros1 was able to efficiently move long-distance into the upper non-inoculated tissue (Fig. 4A and B). Supplementary Fig. S5 shows the pictures of the three independent inoculated plants, as well as the selected leaves, which corresponded to each line. We previously showed that anthocyanin accumulation very precisely correlates with viral load in *Rosea1*-marked viruses (Bedoya et al., 2012). Therefore, in order to make a more quantitative estimate of ZYMV-Ros1 systemic movement in all these plants, we harvested all the aerial tissues above the agroinoculated leaves at 27 dpi and quantified the accumulation of reddish anthocyanins by a spectrophotometric analysis (Fig. 4C and Supplementary Table S3). While anthocyanin accumulation in the DCL1.13i, DCL2.11i and DCL3.10i lines was negligible and indistinguishable from the wild-type plants, the aerial tissues of lines DCL4.9i, DCL2/4.5i and DCL3.10(x)2/4.5i accumulated substantial amounts of these pigments (Fig. 4C). It was noteworthy that the anthocyanin accumulations in

the double DCL2/4.5i and in the triple DCL3.10(x)2/4.5i knock-down lines were 1.8- and 2.9-fold higher, respectively, on average than in the single knock-down DCL4.9i line. Taken together, these results support a crucial role of *DCL4* in restricting the systemic movement of ZYMV in *N. benthamiana* that may be functionally complemented by *DCL2* and *DCL3*. To confirm this result, a similar experiment was conducted with wild-type ZYMV under same experimental conditions. Western blot and RT-qPCR analyses of virus accumulation at 28 dpi in the whole upper non-inoculated tissues confirmed the crucial role of *DCL4* in restricting virus systemic movement (Fig. 4D and E).

## DISCUSSION

The goal of this research was to create a tool to facilitate screening ZYMV resistance in the breeding programs of cucurbit plants. Although the initial aim failed, we were able to generate a convenient experimental system to analyze the contribution of ZYMV genetic determinants and host factors to viral systemic movement, which should ultimately help to understand and develop resistance to infection by this virus.

### A new Mediterranean isolate of ZYMV that mostly resembles a sequence variant from Taiwan

We constructed an infectious clone from a Spanish isolate of ZYMV that infected a zucchini plant. Our clone mostly resembles sequence variant AF127929.2, which has been reported in Taiwan and was isolated in 1993 from sponge gourd (*Luffa cylindrical* Roem.) (Lin et al., 2001). The two variants differ in 517 nucleotide positions (94.6% identity), including the insertion of a U at position 9465, which corresponds to the 3' UTR. Our finding of a 2013 Mediterranean isolate that mostly resembled a 1993 Taiwanese sequence variant, which belong to phylogenetic group A-IV, mainly composed of East Asian isolates (Coutts et al., 2011), supports the easy worldwide dispersion of this virus.

### The ZYMV-mediated expression of Rosea1 does not produce visible anthocyanin accumulation in cucurbit plants

We constructed a recombinant ZYMV clone that expresses *A. majus* R2R3 MYB transcription factor Rosea1 (ZYMV-Ros1, Fig. 1A and Supplementary Fig. S1). This recombinant clone induced the accumulation of reddish anthocyanins in the infected tissues of *N. benthamiana* (Fig. 2 and Supplementary Fig. S3), but not in cucurbitaceous species like

zucchini (Fig. 1B and Supplementary Fig. S2) or melon (Supplementary Fig. S3). Tomato plants engineered to over-express the two *A. majus* transcription factors Rosea1 and Delila under the control of a fruit-specific promoter produced purple tomatoes with high anthocyanin content (Butelli et al., 2008; Su et al., 2016). In plants, anthocyanin biosynthesis is controlled at the transcriptional level by members of three protein families: R2R3 MYB transcription factors, bHLH transcription factors and WD repeat proteins. They interact to form a ternary complex that activates a series of genes that lead to anthocyanin biosynthesis and accumulation in vacuoles (Zhang et al., 2014). We previously showed that the virus-mediated expression of Rosea1 and Delila in tobacco tissues also induces the accumulation of large amounts of anthocyanins in infected tissues (Bedoya et al., 2010). Next we reported that the sole virus-mediated expression of Rosea1 suffices to induce pigment accumulation that is readily detectable to the naked eye in infected tissues in several host plant-virus combinations. This finding suggests that this transcription factor is a convenient marker to visually track plant virus infection and movement (Bedoya et al., 2012). In terms of the size, Rosea1 is only slightly larger than the most conventional reporter gene used in plant virology, green fluorescent protein (GFP) (Tilsner and Oparka, 2010). Although the impact of Rosea1 in recombinant virus fitness is stronger than that of GFP, the stabilities of both markers in the viral genome are similar (Majer et al., 2013). We succeeded in producing a visible reddish pigmentation of the infected tissues in solanaceous plants (*N. benthamiana* or *Nicotiana tabacum* L.), but also in the non-solanaceous *Arabidopsis thaliana* L. using recombinant potyviruses, such as TEV or *Turnip mosaic virus* (TuMV), and also with viruses like *Tobacco mosaic virus* or *Potato virus X* that belong to different families (Bedoya et al., 2012). *Narcissus mosaic virus* (genus *Potexvirus*) has also been shown to induce visible pigment production in *N. benthamiana* plants, when expressing *A. thaliana* R2R3 MYB transcription factor AtMYB75 (PAP1) (Zhang et al., 2013). Lack of pigment accumulation in the tissues of cucurbitaceous plants infected with ZYMV-Ros1 may result from an incompatibility between *A. majus* Rosea1 and the endogenous companion transcription factors of the bHLH and WD repeat types. Not much is known about the flavonoid pathway in cucurbits. Other flavonoids, such as flavone derivatives, have been detected in cucumber (*Cucumis sativus* L.) and melon leaves (Krauze-Baranowska and Cisowski, 2001). Flavonol derivatives have also been reported in the reproductive organs of some cucurbits (Imperato, 1980). Naringenin chalcone is the main flavonoid that accumulates in the fruit rind of some yellow melon varieties (Tadmor et al., 2010; Feder et al., 2015).

Zucchini plants infected with ZYMV-Ros1 showed milder symptoms than those infected with wild-type ZYMV (Fig. 1B and Supplementary Fig. S2). Some leaves in these plants presented a distinctive beautiful pattern that consisted in dark green perinerval stripes on a light green background (Fig. 1B and Supplementary Fig. S2). The possibility that these distinctive symptoms might still arise from some unknown activity of the Rosea1 transcription factor cannot be ruled out.

**ZYMV-Ros1 inefficiently moves long-distance in *N. benthamiana***

According to the anthocyanin production induced by the Rosea1 marker, we observed that ZYMV-Ros1 efficiently accumulated in the agroinoculated tissues of *N. benthamiana* plants, but very few particles from the progeny were able to establish systemic infection foci (Fig. 2 and Supplementary Fig. S4). As an alternative to agroinoculation, we obtained the same result from mechanical inoculation of *N. benthamiana* plants with an extract of ZYMV-Ros1-infected zucchini. It is worth noting that the visual marker was crucial for this observation since very few systemic infection foci kept appearing in the first weeks after inoculation. The Rosea1-induced pigmented foci, which were directly observable without using specialized instrumentation such as a UV lamp (Bedoya et al., 2012), easily attracted our attention. It has been previously described that some ZYMV strains induce latent infection in *N. benthamiana* either systemically or in a limited manner to inoculated tissue (Lesemann et al., 1983; Wang et al., 1992; Desbiez and Lecoq, 1997).

We reasoned that the combination of our recombinant ZYMV-Ros1 virus and the *N. benthamiana* host could represent an excellent experimental system to study the virus genetic determinants and host factors involved in ZYMV systemic movement. *N. benthamiana*, particularly the lineage used in most research laboratories, is susceptible to a large number of plant virus species from very different taxonomic groups. This is most probably because this lineage, which was originally harvested in an extreme habitat of central Australia, is a natural *rdr1* mutant (Bally et al., 2015; Carbonell, 2015). Consequently, this species is frequently adopted as a model plant in many research works into plant viruses. In our system, the amount of viral particles capable of reaching upper non-inoculated tissues was easily determined by monitoring the dark red pigmentation of these tissues. The efficiency of viral systemic movement was also quantified in systemic tissues by counting infection foci or by measuring anthocyanin accumulation by a simple colorimetric analysis of methanol extracts. We previously showed that, for Rosea1-marked viruses, anthocyanin accumulation correlates with viral load in infected tissues (Bedoya et al., 2012). This experimental system should help to

analyze genetic determinants in the virus genome that affect systemic movement. More importantly, this system should allow analyzing the host factors involved in ZYMV systemic movement. In this way, by inoculating knock-out or knock-down *N. benthamiana* mutants, host factors involved in favoring or restricting ZYMV systemic movement could be identified and analyzed. Similarly, by inoculating *N. benthamiana* plants in which the candidate factors from cucurbit species are expressed by stable genetic transformation or by transient expression through *A. tumefaciens* or viral vectors, the host factors that are recruited by the virus to mediate its systemic movement in the natural hosts could be screened. The identification and analysis of all these factors will provide an understanding of the mechanisms that underlie ZYMV systemic movement. These factors may also be used as targets to breed or engineer resistance in cucurbitaceous plants by blocking virus systemic movement.

**_DCL4_ is involved in restricting ZYMV systemic movement in _N. benthamiana_**

Since DCL proteins initiate the antiviral RNA silencing response in plants (Aliyari and Ding, 2009; Zhang et al., 2015), we used our new experimental system, based on ZYMV-Ros1 and *N. benthamiana*, to analyze the effects of *DCL* genes on ZYMV systemic accumulation. *N. benthamiana*, like *A. thaliana*, encodes four DCL type-III RNases (Nakasugi et al., 2013). We took advantage of the availability of a recently generated collection of *N. benthamiana* RNAi transgenic lines, in which the different *DCL* genes were down-regulated (Dadami et al., 2013; Katsarou et al., 2016). To better understand the role of these genes in ZYMV systemic movement, we first analyzed the effect of their down-regulations on ZYMV-Ros1 local multiplication in agroinoculated tissue (Fig. 3 and Supplementary Table S2). Interestingly, local accumulation of ZYMV-Ros1 was reduced (0.6-fold on average) in *DCL3* single knock-down plants compared to that observed in wild-type plants. DCL3, which is primarily involved in antiviral defense against DNA viruses (Akbergenov et al., 2006), but also against RNA viruses as DCL4 surrogate (Deleris et al., 2006; Garcia-Ruiz et al., 2010), could be directly involved in ZYMV-Ros1 genome amplification or cell-to-cell movement or, alternatively, could regulate one or more host factors that favor virus multiplication. DCL3 activity may also have a negative effect on *DCL2* and *DCL4*. In contrast, the single down-regulation of *DCL1*, *DCL2* and *DCL4*, and the double down-regulation of *DCL2* and *DCL4*, had no effect on ZYMV-Ros1 local accumulation, which apparently suggests that these three *DCL* may be dispensable for local antiviral silencing. However in this context, we should consider that, unlike most studies in

which viruses with mutations in silencing suppressors have been used (Ziebell and Carr, 2009), in our system ZYMV-Ros1 expresses a wild-type HC-Pro, which may mask the local antiviral effects of these particular *DCL*, as reported before for TuMV in *A. thaliana* (Garcia-Ruiz et al., 2010). The local accumulation of ZYMV-Ros1 increased (1.75-fold on average) in the triple *DCL2*, *DCL3* and *DCL4* knock-down line compared to wild-type plants. This result suggests that these three antiviral *DCL* genes possess co-operative antiviral activity against ZYMV-Ros1 in inoculated tissue, as previously observed in other plant-virus systems (Garcia-Ruiz et al., 2010; Andika et al., 2015).

Next we analyzed the effect of the DCL down-regulation on ZYMV-Ros1 systemic accumulation in upper non-infiltrated tissues. It is interesting to note that, while the single down-regulation of *DCL4* did not affect ZYMV-Ros1 local multiplication, it had a dramatic effect by favoring virus accumulation in systemic tissue. This favorable effect was not observed in the single *DCL1, DCL2* and *DCL3* knock-down plants (Fig. 4, Supplementary Table S3 and Supplementary Fig. S5). Similar results were obtained using a wild-type ZYMV and analyzing virus systemic accumulation by Western blot (Fig. 4D) or by RT-qPCR (Fig. 4E). Therefore, the observations made for ZYMV-Ros1 are unlikely to be an artifact that resulted from an unexpected activity of the Rosea1 marker. In the case of ZYMV-Ros1, the analysis of the anthocyanin content in upper non-inoculated tissues revealed that virus systemic accumulation was enhanced in the double *DCL2* and *DCL4*, and particularly in triple *DCL2*, *DCL3* and *DCL4* knock-down plants (Fig. 4, Supplementary Table S3 and Supplementary Fig. S5). Taken together, these observations support a critical role of *DCL4* in restricting ZYMV-Ros1 systemic accumulation in *N. benthamiana*, while *DCL2* and *DCL3* may functionally complement *DCL4* in this role. Nonetheless, the specific mechanisms that explain how *DCL4* hinders ZYMV systemic amplification in *N. benthamiana* still need to be determined. While it is conceivable that DCL4 prevents the entry or passage of viruses into the phloem, DCL4 may also restrict the virus from leaving vascular bundles, as reported for suppressor-deficient *Turnip crinkle virus* in *A. thaliana* (Deleris et al., 2006). In this scenario, as 21-nt siRNA duplexes can move long-distance in plants (Dunoyer et al., 2010), the DCL4-dependent 21-nt siRNA duplexes could be the mobile silencing signal generated in inoculated tissue, which spread throughout the plant to prevent ZYMV from accumulating in the upper non-inoculated leaves (Mermigka et al., 2016). In any case, viral systemic movement in plants is a rather complex and prolonged process, and the specific mechanisms by which antiviral silencing blocks viral systemic spread need to be further clarified.

## MATERIALS AND METHODS

### Amplification of ZYMV cDNAs

Total RNA was purified by silica gel chromatography (Zymo Research) from a piece of symptomatic leaf from a zucchini plant (cultivar Scallop) growing in 2013 in Horta de Vera (Valencia, Spain), which showed typical symptoms of viral infection. From this RNA preparation, cDNAs were initially synthesized using RevertAid reverse transcriptase (Thermo Fisher Scientific) and oligodeoxynucleotide primers P1 and P4, designed on the basis of ZYMV GenBank reference sequence variant NC_003224.1. All primers used in this work are described Supplementary Table S1. The two cDNAs were amplified with Phusion high-fidelity DNA polymerase (Thermo Fisher Scientific) and primers P2 and P3, and P5 and P6. New cDNAs corresponding to the 5' and 3' viral ends were amplified by RACE. To amplify the 3' end, we took advantage of the native polyadenilate tail of ZYMV genomic RNA. Using primer P7, we synthesized a cDNA, which was next amplified by two subsequent PCR using primers P8 and P9, and P10 and P11. To amplify the 5' end, we first synthesized a cDNA using primer P12. A polytimidine tail was next added to the 3' end of this cDNA using calf thymus terminal transferase (Thermo Scientific). Finally, the 5' end was amplified in two consecutive PCR using primers P13 and P14, and P15 and P16. All these cDNAs were inserted into EcoRV-digested pBluescript II KS(+) (GeneBank accession number X52327.1) and sequenced. Experimental sequences served to design new primers (P17 to P29, see Supplementary Table S1) to amplify the whole ZYMV genome in three fragments (5', central and 3') by RT-PCR. We applied a nested PCR strategy, in which 1 µl of the first reaction was used as a template for the second reaction. These three ZYMV cDNAs were ligated to EcoRV-digested pBluescript II KS(+) using T4 DNA ligase (Thermo Fisher Scientific), and *Escherichia coli* DH5α electroporated with the products of ligations.

### Construction of ZYMV infectious clones

The cloned cDNAs corresponding to the 5', central and 3' fragments of the Vera isolate of ZYMV were recovered by digestion with the type-IIS restriction enzyme Eco31I (Thermo Fisher Scientific) from the pBluescript II KS(+) derivatives (see above) and assembled (Engler et al., 2009) into the binary vector pG35Z also digested with Eco31I. pG35Z is a binary vector derived from pCLEAN-G181(GenBank accession number EU186083) (Thole et al., 2007) that we constructed as a previous step to assemble the ZYMV full-length clone. The map and sequence of pG35Z is in Supplementary Fig. S6. The resulting

plasmid harboring the full cDNA of the Vera isolate of ZYMV (GenBank accession number KX499498) was named pGZYMV. Using PCR with the Phusion high-fidelity DNA polymerase, digestion with Eco31I and ligation with T4 DNA ligase a cDNA corresponding to the coding region of *A. majus Rosea1* transcription factor (GenBank accession number DQ275529.1) was inserted between NIb and CP cistron (positions 8541 and 8542 of KX499498). This cDNA was flanked with sequences coding for amino acids to complement native NIb/CP proteolytic site that was split in two (see Supplementary Fig. S1). The resulting plasmid was named pGZYMV-Ros1.

**Plant agroinoculation**

*A. tumefaciens* C58C1 harboring the helper plasmid pCLEAN-S48 (Thole et al., 2007) was electroporated with pG35Z (empty plasmid), pGZYMV or pGZYMV-Ros1. Liquid cultures of transformed *A. tumefaciens* were grown to optical density (600 nm) of approximately 1.0. Cells were recovered by centrifugation and resuspended at an optical density (600 nm) of 0.5 in 10 mM MES-NaOH, pH 5.6, 10 mM $MgCl_2$ and 150 µM acetosyringone. Cultures were induced for 3 h at 28ºC and used to agroinoculate zucchini (cultivar MU-CU-16), melon (cultivar Piel de Sapo) or *N. benthamiana* plants (Bedoya and Daròs, 2010). The inbreeding line MU-CU-16 belongs to the Zucchini morphotype of the ssp. pepo of *C. pepo* and was provided by the Cucurbits Breeding Group of the Institute for the Conservation and Breeding of Agricultural Biodiversity, Universitat Politècnica de València (Blanca et al., 2011; Esteras et al., 2012). We agroinoculated 3 days old zucchini, approximately one month old melon plants and 4.5 or 5.5 weeks old *N. benthamiana* plants.

**Western blot analysis**

Infiltrated tissues of *N. benthamiana* plants (5.5 weeks old) were harvested 6 dpi (between 0.45 and 0.89 g depending on the sample) and ground with a mortar and pestle in the presence of liquid $N_2$. Three volumes of buffer TEW (60 mM Tris-HCl, pH 6.8, 2% sodium dodecyl sulfate (SDS), 100 mM dithiothreitol, 10% w/v glycerol and 0.01% bromophenol blue) were added and the extracts incubated at 95ºC for 5 min. Extracts were clarified by centrifugation for 15 min and 40 µl of the supernatants (equivalent to 13 mg of fresh tissue) separated by discontinuous polyacrylamide gel electrophoresis (PAGE) in 12.5% polyacrylamide gels (5% polyacrylamide for the stacking gel) containing 0.05% SDS. Proteins were electroblotted to polyvinylidene fluoride membranes (GE Healthcare), which were blocked for 1 h in 5% non-fat milk in buffer WB (10 mM Tris-HCl, pH 7.5, 154 mM

NaCl and 0.1% w/v Nonidet P40) and incubated overnight at 4°C with an anti ZYMV CP antibody conjugated to alkaline phosphatase (Agdia) at 1:10,000 dilution in 5% non-fat milk in WB. Membranes were washed three times with WB and alkaline phosphatase detected with CSPD (Roche Life Science). Luminescence was recorded and quantified with a LAS-3000 image analyzer (Fujifilm). This protocol was also used to analyze the accumulation of ZYMV CP in upper non-inoculated leaves of *N. benthamiana DCL* knock-down plants. In this case the whole plant aerial tissues were harvested at 28 dpi, frozen, ground and mixed. Aliquots of approximately 1 g of frozen tissue were sampled for the analysis.

**Anthocyanins extraction and quantification**

*N. benthamiana* wild-type and *DCL* knock-down (Dadami et al., 2013Dadami et al., 2013; Katsarou et al., 2016) plants (5 weeks old) were agroinoculated in three leaves with ZYMV-Ros1, as indicated above. The whole aerial parts of the plants were harvested at 27 dpi and frozen at -80ºC. Frozen tissues were ground and aliquots of approximately 1 g were homogenized with 10 volumes of methanol containing 1% HCl using a Polytron (Kinematica). Extracts were incubated on ice for 1 h with occasional vortexing. Extracts were clarified by centrifugation and an aliquot of the supernatant was further diluted 1:5 in 1% HCl in methanol (final ratio tissue:extraction solution 1:50). Anthocyanin concentration was quantified by measuring absorbance at 543 nm with a spectrophotometer (Biowave II, WPA) using a 1 cm path cuvette.

**RT-qPCR analysis of ZYMV RNA**

RNA preparations were purified from *N. benthamiana* tissue samples using the RNeasy Plant Mini Kit (Qiagen) and quantified using a NanoDrop ND-1000 spectrophotomer. cDNAs were synthesized in 20 µl reactions including 100 ng of total RNA, 50 U RevertAid reverse transcriptase and 5 pmol of primer P30. Two µl of the products of these reactions were subjected to 20 µl qPCR amplification reactions by triplicate using the Maxima SYBR Green/ROX qPCR Master Mix (Thermo Scientific) and 6 pmol primers P31 and P32 in a StepOnePlus Real-Time PCR System (Applied Biosystems). The amount of ZYMV RNA molecules present in 100 ng of RNA preparation was calculated from a calibration line obtained in the same condition with an RNA standard corresponding to ZYMV 3' genome fragment (from position 8542 to 9592 of KX499498) obtained by *in vitro* run off transcription and quantified by spectrophotometric analysis. StepOne Software v.2.2.2 (Applied Biosystems) was used to analyze the data.

## ACKNOWLEDGEMENTS

We thank Verónica Aragonés for excellent technical assistance. This work was supported by the Spanish Ministerio de Economía y Competitividad (MINECO) through grants BIO2014-54269-R and AGL2013-49919-EXP, and by the Greek Ministry for Education and Religious Affairs (Program Aristeia II, 4499, ViroidmiR; ESPA 2007-2013). A.C. was supported by an Individual Fellowship from the European Union's Horizon 2020 research and innovation programme under the Marie Sklodowska-Curie grant agreement No. 655841.

## LITERATURE CITED

Akbergenov, R., Si-Ammour, A., Blevins, T., Amin, I., Kutter, C., Vanderschuren, H., Zhang, P., Gruissem, W., Meins, F., Jr., Hohn, T., and Pooggin, M. M. 2006. Molecular characterization of geminivirus-derived small RNAs in different plant species. Nucleic Acids Res. 34:462-471.

Aliyari, R., and Ding, S. W. 2009. RNA-based viral immunity initiated by the Dicer family of host immune receptors. Immunol. Rev. 227:176-188.

Andika, I. B., Maruyama, K., Sun, L., Kondo, H., Tamada, T., and Suzuki, N. 2015. Differential contributions of plant Dicer-like proteins to antiviral defences against potato virus X in leaves and roots. Plant J. 81:781-793.

Bally, J., Nakasugi, K., Jia, F., Jung, H., Ho, S. Y., Wong, M., Paul, C. M., Naim, F., Wood, C. C., Crowhurst, R. N., Hellens, R. P., Dale, J. L., and Waterhouse, P. M. 2015. The extremophile Nicotiana benthamiana has traded viral defence for early vigour. Nat. Plants 1:15165.

Bedoya, L., Martínez, F., Rubio, L., and Daròs, J. A. 2010. Simultaneous equimolar expression of multiple proteins in plants from a disarmed potyvirus vector. J. Biotechnol. 150:268-275.

Bedoya, L. C., and Daròs, J. A. 2010. Stability of *Tobacco etch virus* infectious clones in plasmid vectors. Virus Res. 149:234-240.

Bedoya, L. C., Martínez, F., Orzáez, D., and Daròs, J. A. 2012. Visual tracking of plant virus infection and movement using a reporter MYB transcription factor that activates anthocyanin biosynthesis. Plant Physiol. 158:1130-1138.

508 Blanca, J., Canizares, J., Roig, C., Ziarsolo, P., Nuez, F., and Picó, B. 2011. Transcriptome
509 characterization and high throughput SSRs and SNPs discovery in *Cucurbita pepo*
510 (Cucurbitaceae). BMC Genomics 12:104.
511 Butelli, E., Titta, L., Giorgio, M., Mock, H. P., Matros, A., Peterek, S., Schijlen, E. G., Hall,
512 R. D., Bovy, A. G., Luo, J., and Martin, C. 2008. Enrichment of tomato fruit with
513 health-promoting anthocyanins by expression of select transcription factors. Nat.
514 Biotechnol. 26:1301-1308.
515 Carbonell, A. 2015. Trading defence for vigour. Nat Plants 1:15174.
516 Carbonell, A., and Carrington, J. C. 2015. Antiviral roles of plant ARGONAUTES. Current
517 Opin. Plant Biol. 27:111-117.
518 Coutts, B. A., Kehoe, M. A., Webster, C. G., Wylie, S. J., and Jones, R. A. 2011. Zucchini
519 yellow mosaic virus: biological properties, detection procedures and comparison of coat
520 protein gene sequences. Arch. Virol. 156:2119-2131.
521 Csorba, T., Kontra, L., and Burgyàn, J. 2015. Viral silencing suppressors: tools forged to fine-
522 tune host-pathogen coexistence. Virology 479-480:85-103.
523 Dadami, E., Boutla, A., Vrettos, N., Tzortzakaki, S., Karakasilioti, I., and Kalantidis, K. 2013.
524 DICER-LIKE 4 but not DICER-LIKE 2 may have a positive effect on potato spindle
525 tuber viroid accumulation in *Nicotiana benthamiana*. Mol. Plant 6:232-234.
526 Deleris, A., Gallego-Bartolome, J., Bao, J., Kasschau, K. D., Carrington, J. C., and Voinnet,
527 O. 2006. Hierarchical action and inhibition of plant Dicer-like proteins in antiviral
528 defense. Science 313:68-71.
529 Desbiez, C., and Lecoq, H. 1997. Zucchini yellow mosaic virus. Plant Pathology 46:809-829.
530 Dunoyer, P., Schott, G., Himber, C., Meyer, D., Takeda, A., Carrington, J. C., and Voinnet,
531 O. 2010. Small RNA duplexes function as mobile silencing signals between plant cells.
532 Science 328:912-916.
533 Engler, C., Gruetzner, R., Kandzia, R., and Marillonnet, S. 2009. Golden gate shuffling: a
534 one-pot DNA shuffling method based on type IIs restriction enzymes. PLoS One
535 4:e5553.
536 Esteras, C., Gómez, P., Monforte, A. J., Blanca, J., Vicente-Dólera, N., Roig, C., Nuez, F.,
537 and Picó, B. 2012. High-throughput SNP genotyping in *Cucurbita pepo* for map
538 construction and quantitative trait *loci* mapping. BMC Genomics 13:80.
539 Feder, A., Burger, J., Gao, S., Lewinsohn, E., Katzir, N., Schaffer, A. A., Meir, A.,
540 Davidovich-Rikanati, R., Portnoy, V., Gal-On, A., Fei, Z., Kashi, Y., and Tadmor, Y.

2015. A kelch domain-containing F-box coding gene negatively regulates flavonoid accumulation in muskmelon. Plant Physiol. 169:1714-1726.

Garcia-Ruiz, H., Takeda, A., Chapman, E. J., Sullivan, C. M., Fahlgren, N., Brempelis, K. J., and Carrington, J. C. 2010. *Arabidopsis* RNA-dependent RNA polymerases and Dicer-like proteins in antiviral defense and small interfering RNA biogenesis during *Turnip mosaic virus* infection. Plant Cell 22:481-496.

Hamilton, A. J., and Baulcombe, D. C. 1999. A species of small antisense RNA in posttranscriptional gene silencing in plants. Science 286:950-952.

Imperato, F. 1980. Five plants of the family Cucurbitaceae with flavonoid patterns of pollens different from those of corresponding stigmas. Experientia 36:1136-1137.

Katsarou, K., Mavrothalassiti, E., Dermauw, W., Van Leeuwen, T., and Kalantidis, K. 2016. Combined activity of DCL2 and DCL3 is crucial in the defense against *Potato spindle tuber viroid*. PLoS Pathog. 12:e1005936.

Krauze-Baranowska, M., and Cisowski, W. 2001. Flavonoids from some species of the genus *Cucumis*. Biochem. Syst. Ecol. 29:321-324.

Lecoq, H., and Desbiez, C. 2012. Viruses of cucurbit crops in the Mediterranean region: an ever-changing picture. Adv. Virus Res. 84:67-126.

Lesemann, D. E., Makkouk, K. M., Koenig, R., and Natafji Samman, E. 1983. Natural infection of cucumbers by zucchini yellow mosaic virus in Lebanon. Phytopathologische Zeitschrift 108:304-313.

Lin, S. S., Hou, R. F., and Yeh, S. D. 2001. Complete genome sequence and genetic organization of a Taiwan isolate of *Zucchini yellow mosaic virus*. Bot. Bul. Acad. Sin. 42:243-250.

Lisa, V., Boccardo, G., D'Agostino, G., Dellavalle, G., and D'Aquilio, M. 1981. Characterization of a potyvirus that causes zucchini yellow mosaic. Phytopathology 71:667-672.

Majer, E., Daròs, J. A., and Zwart, M. P. 2013. Stability and fitness impact of the visually discernible Rosea1 marker in the Tobacco etch virus genome. Viruses 5:2153-2168.

Mermigka, G., Verret, F., and Kalantidis, K. 2016. RNA silencing movement in plants. J. Integr. Plant Biol. 58:328-342.

Nakasugi, K., Crowhurst, R. N., Bally, J., Wood, C. C., Hellens, R. P., and Waterhouse, P. M. 2013. *De novo* transcriptome sequence assembly and analysis of RNA silencing genes of *Nicotiana benthamiana*. PLoS One 8:e59534.

574 Revers, F., and García, J. A. 2015. Molecular biology of potyviruses. Adv. Virus Res. 92:101-
575 199.
576 Su, X., Xu, J., Rhodes, D., Shen, Y., Song, W., Katz, B., Tomich, J., and Wang, W. 2016.
577 Identification and quantification of anthocyanins in transgenic purple tomato. Food
578 Chem. 202:184-188.
579 Tadmor, Y., Burger, J., Yaakov, I., Feder, A., Libhaber, S. E., Portnoy, V., Meir, A., Tzuri,
580 G., Sa'ar, U., Rogachev, I., Aharoni, A., Abeliovich, H., Schaffer, A. A., Lewinsohn, E.,
581 and Katzir, N. 2010. Genetics of flavonoid, carotenoid, and chlorophyll pigments in
582 melon fruit rinds. J. Agric. Food Chem. 58:10722-10728.
583 Thole, V., Worland, B., Snape, J. W., and Vain, P. 2007. The pCLEAN dual binary vector
584 system for *Agrobacterium*-mediated plant transformation. Plant Physiol. 145:1211-
585 1219.
586 Tilsner, J., and Oparka, K. J. 2010. Tracking the green invaders: advances in imaging virus
587 infection in plants. Biochem. J. 430:21-37.
588 Wang, H. L., Gonsalves, D., Provvidenti, R., and Zitter, T. A. 1992. Comparative biological
589 and serological properties of four strains of zucchini yellow mosaic virus. Plant Dis.
590 76:530-535.
591 Wang, X. B., Wu, Q., Ito, T., Cillo, F., Li, W. X., Chen, X., Yu, J. L., and Ding, S. W. 2010.
592 RNAi-mediated viral immunity requires amplification of virus-derived siRNAs in
593 Arabidopsis thaliana. Proc. Natl. Acad. Sci. USA 107:484-489.
594 Wu, H. W., Lin, S. S., Chen, K. C., Yeh, S. D., and Chua, N. H. 2010. Discriminating
595 mutations of HC-Pro of *Zucchini yellow mosaic virus* with differential effects on small
596 RNA pathways involved in viral pathogenicity and symptom development. Mol. Plant-
597 Microbe Interact. 23:17-28.
598 Zhang, C., Wu, Z., Li, Y., and Wu, J. 2015. Biogenesis, function, and applications of virus-
599 derived small RNAs in plants. Front. Microbiol. 6:1237.
600 Zhang, H., Wang, L., Hunter, D., Voogd, C., Joyce, N., and Davies, K. 2013. A Narcissus
601 mosaic viral vector system for protein expression and flavonoid production. Plant
602 Methods 9:28.
603 Zhang, Y., Butelli, E., and Martin, C. 2014. Engineering anthocyanin biosynthesis in plants.
604 Current Opin. Plant Biol. 19:81-90.
605 Ziebell, H., and Carr, J. P. 2009. Effects of dicer-like endoribonucleases 2 and 4 on infection
606 of *Arabidopsis thaliana* by cucumber mosaic virus and a mutant virus lacking the 2b
607 counter-defence protein gene. J. Gen. Virol. 90:2288-2292.

608

609 **LEGENDS TO THE FIGURES**

610

611 **Fig. 1.** Symptoms induced by ZYMV and ZYMV-Ros1 in zucchini plants. **A,** Schematic
612 representation of the ZYMV genome. Lines represent the 5' and 3' untranslated regions
613 (UTR) and boxes represent the different viral cistrons as indicated. In ZYMV-Ros1, a cDNA
614 that codes for *A. majus* Rosea1 was inserted between cistrons NIb and CP. The cDNA
615 included sequences that corresponded to extra amino and carboxy terminal peptides, as
616 indicated, to mediate proteolytic release from the polyprotein. **B,** Pictures of representative
617 zucchini plants agroinoculated with the empty binary plasmid, ZYMV or ZYMV-Ros1. To
618 better appreciate symptoms, a picture of selected leaves is also shown. All the pictures were
619 taken at 21 dpi. **C,** Western blot analysis of ZYMV CP accumulation in upper non-inoculated
620 tissues of three independent plants agroinoculated with the empty plasmid (lanes 1 to 3), wild-
621 type ZYMV (lanes 4 to 6) and ZYMV-Ros1 (lanes 7 to 9) at 15 dpi. The position and size
622 (expressed in kDa) of marker proteins are indicated at the left of the panel. **D,** Bar graph
623 representing the average ZYMV CP accumulation, quantified as luminescence arbitrary units
624 (AU) by Western blot, in the upper non-inoculated tissues of the previously described (panel
625 C) zucchini plants. Error bars represent the standard error median.

626

627 **Fig. 2.** ZYMV-Ros1 suboptimally moves long-distance in *N. benthamiana*. **A,** Pictures were
628 taken at 7 dpi and are representative of leaves agroinoculated with the empty plasmid, ZYMV
629 or ZYMV-Ros1. **B,** Comparison of systemic leaves from three *N. benthamiana* plants
630 agroinoculated with the empty binary plasmid or ZYMV-Ros1. Arrows indicate the
631 pigmented infectious foci induced by ZYMV-Ros1 in systemic leaves. The picture was taken
632 at 21 dpi.

633

634 **Fig. 3.** Accumulation of ZYMV-Ros1 in the agroinoculated tissues of wild-type *N.*
635 *benthamiana* plants and the lines down-regulated in different *DCL* genes. **A,** Triplicate
636 Western blot analysis of ZYMV CP using a specific antibody conjugated to alkaline
637 phosphatase and a luminogenic reaction. Proteins were separated by SDS-PAGE. Lanes 1 and
638 2, non-inoculated and infected wild-type plants, respectively; lanes 3 to 8, infected *DCL*
639 down-regulated lines, as indicated. The position and size (in kDa) of marker is indicated at the
640 left of the panel. **B,** Bar graph of the average ZYMV CP accumulation, quantified as
641 luminescence AU, in the agroinoculated tissues of three independent *N. benthamiana* plants

642 that corresponded to the wild-type or *DCL* down-regulated lines, as indicated. Tissue from a
643 non-inoculated wild-type plant was also analyzed as a control. Error bars represent the
644 standard error median.
645
646 **Fig. 4.** ZYMV moves long-distance more efficiently in the *N. benthamiana* plants in which
647 *DCL4* is down-regulated. **A,** Pictures of the *N. benthamiana* plants that corresponded to the
648 wild-type and *DCL* knock-down lines, as indicated, and agroinoculated with ZYMV-Ros1.
649 Pictures were taken at 27 dpi. **B,** Pictures of selected leaves of the plants shown in panel A. **C,**
650 Bar graph representing the average anthocyanin accumulation, measured as absorbance at 543
651 nm, in the aerial tissues of three wild-type and *DCL* knock-down *N. benthamiana* plants, as
652 indicated. The average background absorbance of three wild-type non-inoculated controls was
653 subtracted. **D and E,** Bar graphs representing the average ZYMV CP accumulation quantified
654 by Western blot analysis (D), and the average ZYMV RNA accumulation quantified by RT-
655 qPCR (E), in the upper non-inoculated leaves of three wild-type and *DCL* knock-down *N.*
656 *benthamiana* plants agroinoculated with wild-type ZYMV. Tissues were harvested 28 dpi.
657 Error bars indicated standard error median.

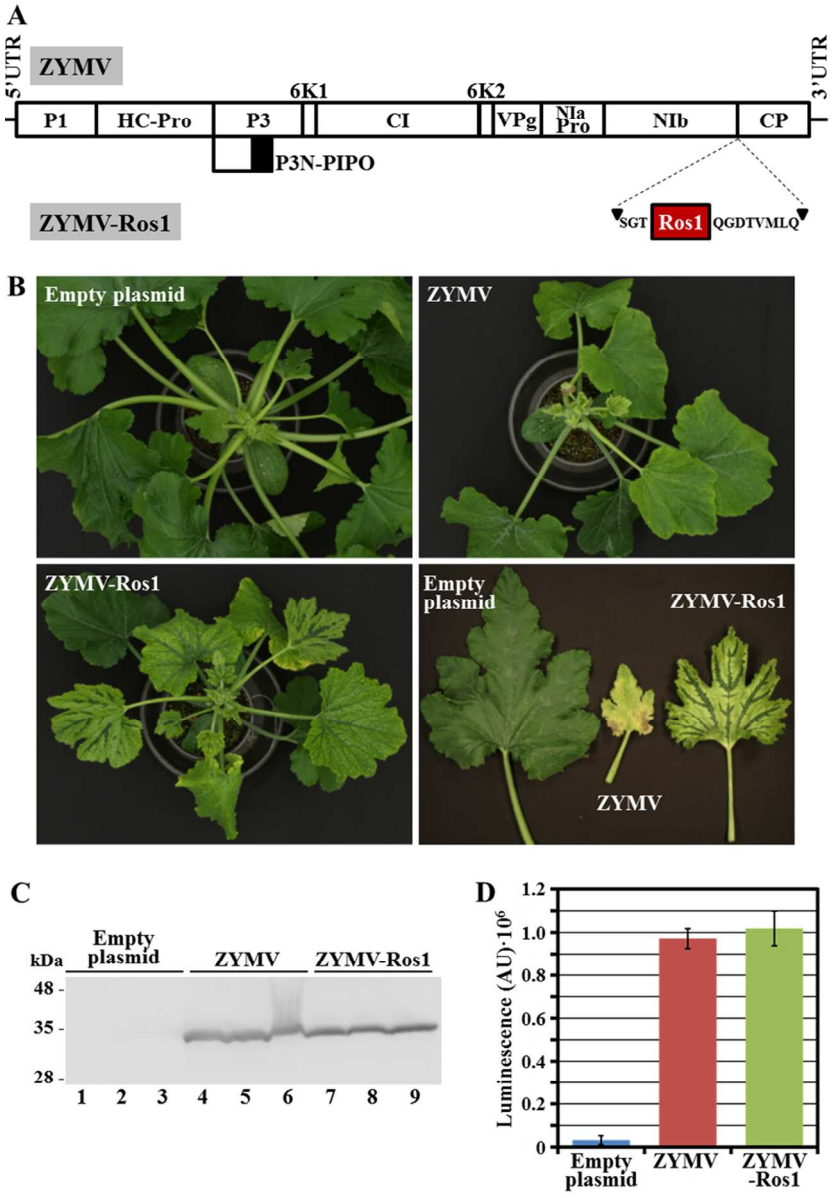


Fig. 1. Symptoms induced by ZYMV and ZYMV-Ros1 in zucchini plants. A, Schematic representation of the ZYMV genome. Lines represent the 5' and 3' untranslated regions (UTR) and boxes represent the different viral cistrons as indicated. In ZYMV-Ros1, a cDNA that codes for A. majus Rosea1 was inserted between cistrons NIb and CP. The cDNA included sequences that corresponded to extra amino and carboxy terminal peptides, as indicated, to mediate proteolytic release from the polyprotein. B, Pictures of representative zucchini plants agroinoculated with the empty binary plasmid, ZYMV or ZYMV-Ros1. To better appreciate symptoms, a picture of selected leaves is also shown. All the pictures were taken at 21 dpi. C, Western blot analysis of ZYMV CP accumulation in upper non-inoculated tissues of three independent plants agroinoculated with the empty plasmid (lanes 1 to 3), wild-type ZYMV (lanes 4 to 6) and ZYMV-Ros1 (lanes 7 to 9) at 15 dpi. The position and size (expressed in kDa) of marker proteins are indicated at the left of the panel. D, Bar graph representing the average ZYMV CP accumulation, quantified as luminescence arbitrary units (AU) by Western blot, in the upper non-inoculated tissues of the previously described (panel C) zucchini plants. Error bars represent the standard error median.

Fig. 1
80x116mm (300 x 300 DPI)

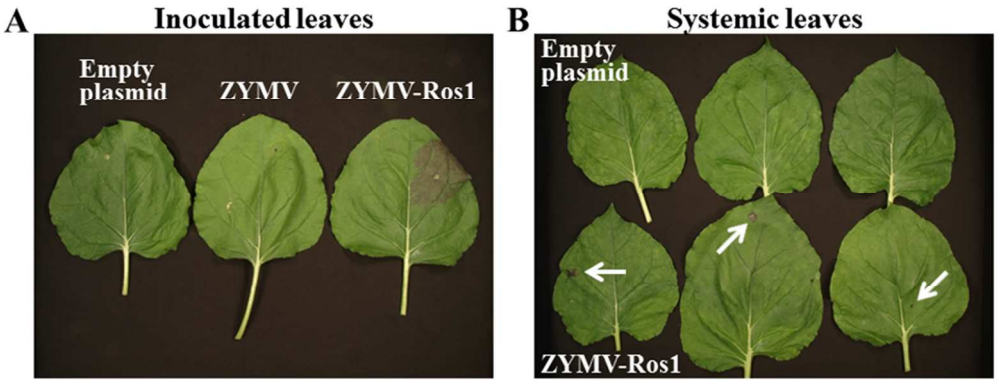


Fig. 2. ZYMV-Ros1 suboptimally moves long-distance in N. benthamiana. A, Pictures were taken at 7 dpi and are representative of leaves agroinoculated with the empty plasmid, ZYMV or ZYMV-Ros1. B, Comparison of systemic leaves from three N. benthamiana plants agroinoculated with the empty binary plasmid or ZYMV-Ros1. Arrows indicate the pigmented infectious foci induced by ZYMV-Ros1 in systemic leaves. The picture was taken at 21 dpi.
Fig. 2
80x29mm (300 x 300 DPI)

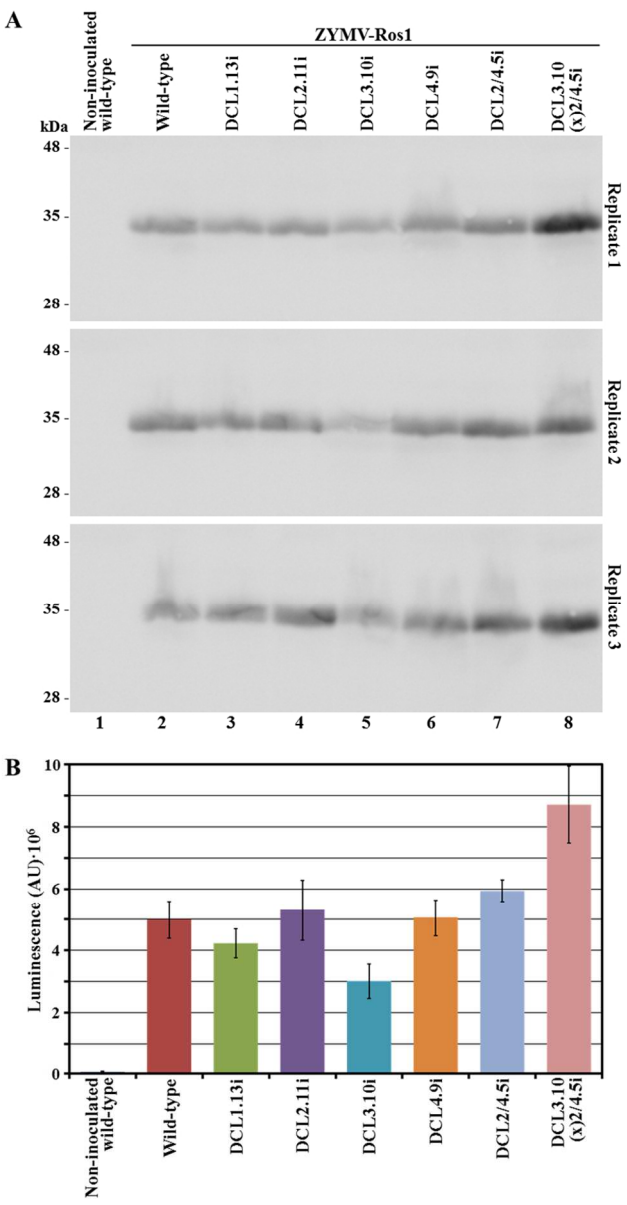


Fig. 3. Accumulation of ZYMV-Ros1 in the agroinoculated tissues of wild-type N. benthamiana plants and the lines down-regulated in different DCL genes. A, Triplicate Western blot analysis of ZYMV CP using a specific antibody conjugated to alkaline phosphatase and a luminogenic reaction. Proteins were separated by SDS-PAGE. Lanes 1 and 2, non-inoculated and infected wild-type plants, respectively; lanes 3 to 8, infected DCL down-regulated lines, as indicated. The position and size (in kDa) of marker is indicated at the left of the panel. B, Bar graph of the average ZYMV CP accumulation, quantified as luminescence AU, in the agroinoculated tissues of three independent N. benthamiana plants that corresponded to the wild-type or DCL down-regulated lines, as indicated. Tissue from a non-inoculated wild-type plant was also analyzed as a control. Error bars represent the standard error median.

Fig. 3
80x138mm (300 x 300 DPI)

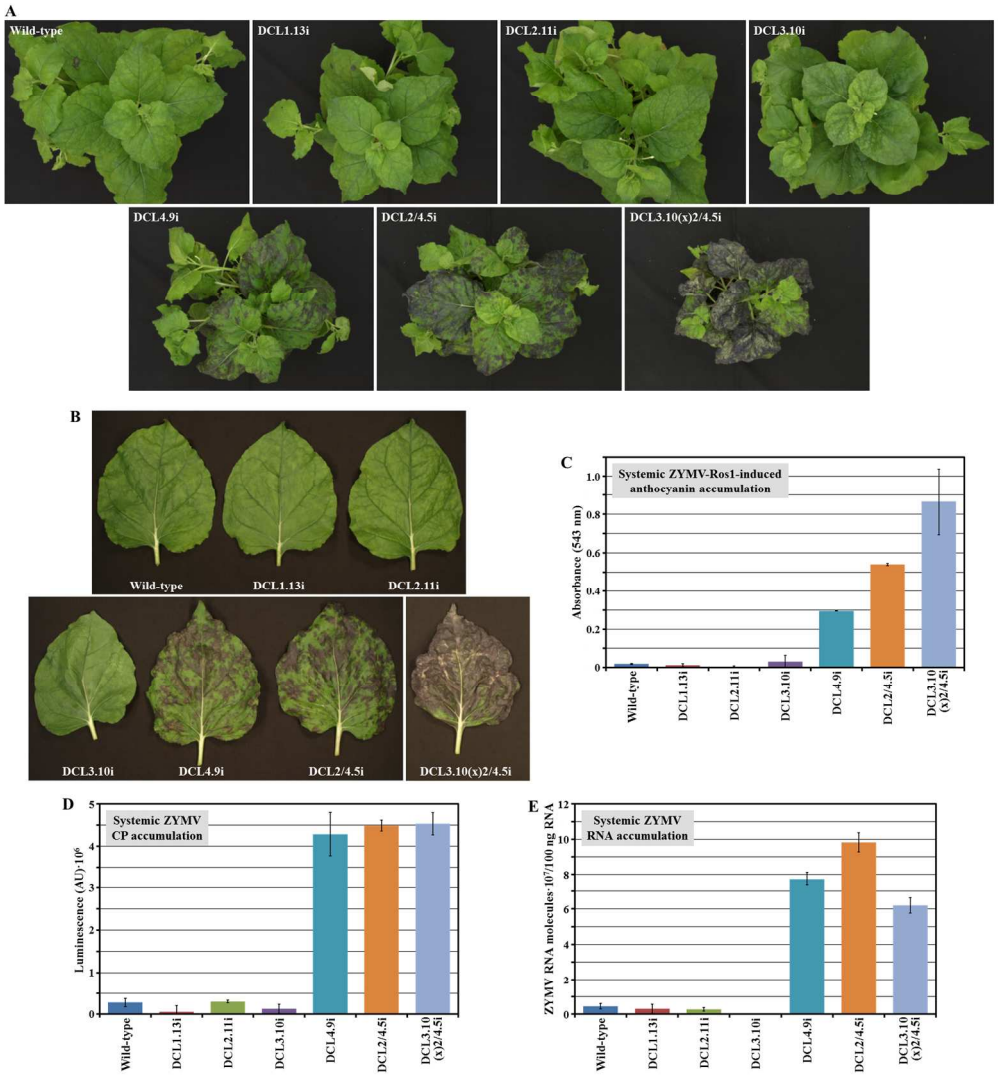


Fig. 4. ZYMV moves long-distance more efficiently in the N. benthamiana plants in which DCL4 is down-regulated. A, Pictures of the N. benthamiana plants that corresponded to the wild-type and DCL knock-down lines, as indicated, and agroinoculated with ZYMV-Ros1. Pictures were taken at 27 dpi. B, Pictures of selected leaves of the plants shown in panel A. C, Bar graph representing the average anthocyanin accumulation, measured as absorbance at 543 nm, in the aerial tissues of three wild-type and DCL knock-down N. benthamiana plants, as indicated. The average background absorbance of three wild-type non-inoculated controls was subtracted. D and E, Bar graphs representing the average ZYMV CP accumulation quantified by Western blot analysis (D), and the average ZYMV RNA accumulation quantified by RT-qPCR (E), in the upper non-inoculated leaves of three wild-type and DCL knock-down N. benthamiana plants agroinoculated with wild-type ZYMV. Tissues were harvested 28 dpi. Error bars indicated standard error median.

Fig. 4
170x183mm (300 x 300 DPI)

## SUPPLEMENTARY TABLE S1

**Supplementary Table S1.** The oligonucleotides used to amplify ZYMV cDNAs by RT-PCR or 5' and 3' RACE.

| Primer name | Sequence[1] | Type of reaction | Purpose of reaction |
|---|---|---|---|
| P1 | TGTTAATATCAAAGTCAATTGTGAG | RT | Amplification internal cDNA |
| P2 | GTTGCTCTGGCTGAAGTTCTTGTGG | PCR | |
| P3 | TATCGTCCTCCAAGCTCTCAATATC | | |
| P4 | GCGATTTTACTAGGTTGCCATAGCC | RT | Amplification internal cDNA |
| P5 | GCATTTATATGGTGTGGAGCCTGAG | PCR | |
| P6 | GTTGAGTCCATGTGAGATCGTCAAG | | |
| P7 | CCAGTGAGCAGAGTGACGAGGACTCGAGCTCAAG CTTTTTTTTTTTTTTTTTVN[2] | RT | 3' RACE |
| P8 | TTGTTTGGCCTTGATGGAAATG | 1st PCR | |
| P9 | CCAGTGAGCAGAGTGACG | | |
| P10 | GCCACCACTAGCGAAGACACTG | 2nd nested PCR | |
| P11 | GAGGACTCGAGCTCAAGC | | |
| P12 | TGAAGAAGTTGTTCAGAATGTC | RT | 5' RACE |
| P13 | GAGTGACGAGGACTCGAGCTCAAGCAAAAAAAA AAAAAAAAAABN[3] | 1st PCR | |
| P14 | GCTTTTGTTTGATTGCATCAAC | | |
| P15 | GAGTGACGAGGACTCGAGCTCAAGC | 2nd nested PCR | |
| P16 | CTTGGACTCATGCCTGTAGTATG | | |
| P17 | CACAGTATTAGACATTTGTAACACC | RT | Amplification 5' fragment ZYMV genome |
| P18 | AAATTAAAACAAATCACAAAG | 1st PCR | |
| P19 | AAGAGAATACCAAACACACGTTCAC | | |
| P20 | GGCG*GGTCTC*GGAGGAAATTAAAACAAATCACAA AGACTACAG[4] | 2nd nested PCR | |
| P21 | CCGC*GGTCTC*CGGTATATAATGTCGCTGTAACACC G | | |
| P22 | CACCATGCCAAGACCTGACTAGAAG | RT | Amplification central fragment ZYMV genome |
| P23 | GATTTTTGCGCGGTGTTACAGCGAC | 1st PCR | |
| P24 | TGTACCATTGTTTTTCCTGAAGAGG | | |
| P25 | GGCG*GGTCTC*GTACCTTGTGAACGTGTGTTTGG | 2nd nested PCR | |
| P26 | CCGC*GGTCTC*CTGCCCATTAGTAATGATTATCGGC C | | |
| P7 | See above | RT | Amplification 3' fragment ZYMV genome |
| P27 | GGCG*GGTCTC*GGGCACCTCTTCAGGAAAAACAAT GG | 1st PCR | |
| P28 | TTTTTTAGGCTTGCAAACGGAG | | |
| P27 | See above | 2nd heminested PCR | |
| P29 | CCGC*GGTCTC*CTTTTAGGCTTGCAAACGGAGTCTA ATC | | |
| P30 | AGGCTTGCAAACGGAGTCTAA | RT | Quantification ZYMV RNA |
| P31 | CTGCCACGCGTGAAAGG | qPCR | |
| P32 | CCGGTTTATATTCCAGCAAATGA | | |

[1]From 5' to 3' end.
[2]V is A, C or G and N is A, C, G or T.
[3]B is C, G or T.
[4]Eco31I recognition and cleavage sites are in italics and underlined, respectively.

**SUPPLEMENTARY TABLE S2**

**Supplementary Table S2.** Accumulation of ZYMV CP in agroinoculated tissues of the wild-type *N. benthamiana* plants and lines down-regulated in different *DCL* genes. Quantitative data were obtained by a Western blot analysis with a specific polyclonal antibody conjugated to alkaline phosphatase and luminescent detection (see Supplementary Fig. S5).

| Plants | ZYMV CP amount (luminescence arbitrary units)[1] | | | Average | Standard error median |
|---|---|---|---|---|---|
| | Replicate 1 | Replicate 2 | Replicate 3 | | |
| Wild-type[2] | 48142 | 87773 | 39815 | 58576.7 | 14794.8 |
| Wild-type | 4036630 | 6094050 | 4831809 | 4987496.3 | 599005.6 |
| DCL1.13i | 3404372 | 5033826 | 4252287 | 4230161.7 | 470512.9 |
| DCL2.11i | 3871764 | 4865003 | 7172089 | 5302952.0 | 977562.6 |
| DCL3.10i | 2777713 | 2192118 | 4054795 | 3008208.7 | 549920.5 |
| DCL4.9i | 3960995 | 5262727 | 5941922 | 5055214.7 | 581181.0 |
| DCL2/4.5i | 5371757 | 6579362 | 5882827 | 5944648.7 | 349973.3 |
| DCL3.10 (x)2/4.5i | 10936518 | 6679362 | 8532089 | 8715989.7 | 1232370.2 |

[1]Background luminescences of 3443482, 3450638 and 3467911 were subtracted from the measurements of replicates 1, 2 and 3, respectively.
[2]Non-agroinoculated control.

**SUPPLEMENTARY TABLE S3**

**Supplementary Table S3.** Anthocyanin accumulation in systemic tissues of *N. benthamiana* plants agroinoculated with ZYMV-Ros1. Plants corresponded to wild-type and the lines down-regulated in different *DCL* genes.

| Plants | Anthocyanin accumulation (absorbance 543 nm)[1] | | | Average | Standard error median |
|---|---|---|---|---|---|
| | Plant 1 | Plant 2 | Plant 3 | | |
| Wild-type | 0.023 | 0.013 | 0.020 | 0.019 | 0.003 |
| DCL1.13i | 0.002 | 0.005 | 0.028 | 0.012 | 0.008 |
| DCL2.11i | 0.010 | 0.008 | -0.014 | 0.001 | 0.008 |
| DCL3.10i | 0.092 | -0.017 | 0.019 | 0.031 | 0.032 |
| DCL4.9i | 0.296 | 0.298 | 0.293 | 0.296 | 0.001 |
| DCL2/4.5i | 0.537 | 0.531 | 0.552 | 0.540 | 0.006 |
| DCL3.10 (x)2/4.5i | 0.551 | 0.902 | 1.143 | 0.865 | 0.172 |

[1]A background absorbance of 0.095 (average measure for three wild-type non-inoculated control plants) was subtracted.

## SUPPLEMENTARY FIGURE S1

**>Rosea1 cDNA from *A. majus* with 5′ and 3′ extra sequences**

TCTGGCACA**ATGGAAAAGAATTGTCGTGGAGTGAGAAAAGGTACTTGGACCAAAGAAGAAGACACTCTCTTGAGG**
**CAATGTATAGAAGAGTATGGTGAAGGGAAATGGCATCAAGTTCCACACAGAGCAGGGTTGAACCGGTGTAGGAAG**
**AGTTGCAGGCTGAGGTGGTTGAATTATCTGAGGCCAAATATCAAAAGAGGTCGGTTTTCGAGAGATGAAGTGGAC**
**CTAATTGTGAGGCTTCATAAGCTGTTGGGTAACAAATGGTCGCTGATTGCTGGTAGAATTCCTGGAAGGACAGCT**
**AATGACGTGAAGAACTTTTGGAATACTCATGTGGGGAAGAATTTAGGCGAGGATGGAGAACGATGCCGGAAAAAT**
**GTTATGAACACAAAAACCATTAAGCTGACTAATATCGTAAGACCCCGAGCTCGGACCTTCACCGGATTGCACGTT**
**ACTTGGCCGAGAGAAGTCGGAAAAACCGATGAATTTTCAAATGTCCGGTTAACAACTGATGAGATTCCAGATTGT**
**GAGAAGCAAACGCAATTTTACAATGATGTTGCGTCGCCACAAGATGAAGTTGAAGACTGCATTCAGTGGTGGAGT**
**AAGTTGCTAGAAACAACGGAGGATGGGGAATTAGGAAACCTATTCGAGGAGGCCCAACAAATTGGAAAT**CAGGGA
GATACTGTGATGCTTCAA

**Supplementary Fig. S1.** Sequence of the cDNA that corresponded to the coding region of *A. majus* Rosea1 (GenBank accession number DQ275529.1) that was inserted between cistrons NIb and CP (between positions 8541 and 8542) of the Vera isolated of ZYMV (GenBank accession number KX499498) to obtain recombinant clone ZYMV-Ros1. The cDNA of Rosea1 was flanked at 5’ and 3’ by extra nucleotides (underlined) which encode peptides that complement the two parts of the split NIb/CP proteolytic site.

**SUPPLEMENTARY FIGURE S2**


**Supplementary Fig. S2.** Zucchini plants agroinoculated with the empty binary plasmid, with ZYMV or with ZYMV-Ros1. Pictures show three independent plants inoculated with each *A. tumefaciens* culture and selected leaves from each plant to better appreciate symptoms. All the pictures were taken on 21 dpi. Close-ups of some of these pictures were used to create Fig. 1.

**SUPPLEMENTARY FIGURE S3**

**Supplementary Fig. S3.** Pictures of melon plants agroinoculated with ZYMV-Ros1 (17 dpi).

**SUPPLEMENTARY FIGURE S4**

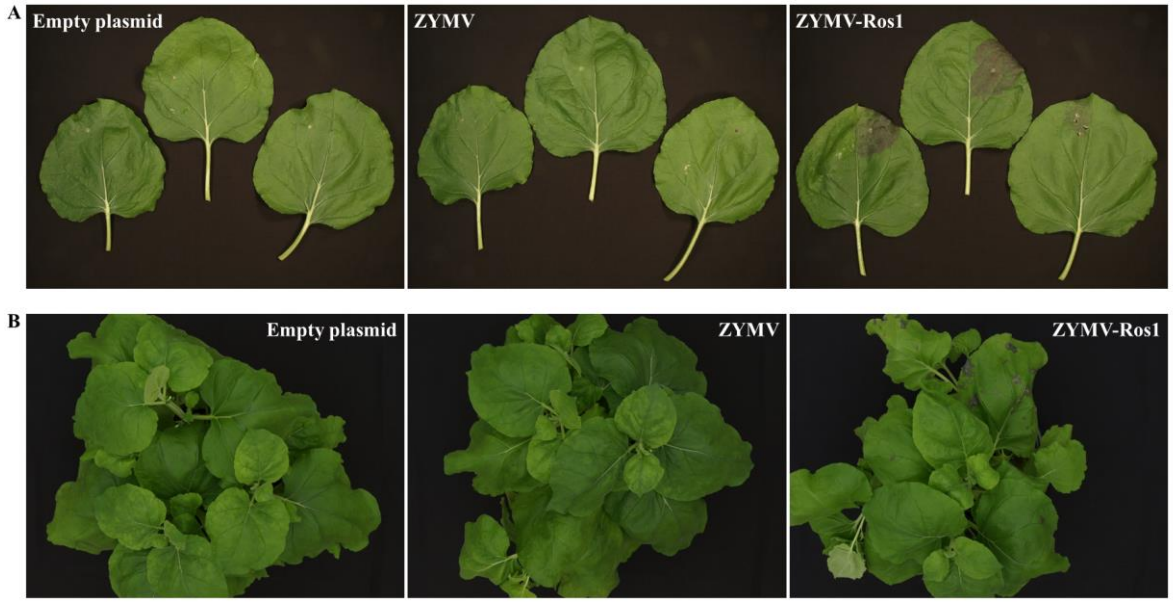


**Supplementary Fig. S4.** ZYMV-Ros1 very inefficiently moves long-distance in *N. benthamiana*. **A,** Sets of three *N. benthamiana* leaves agroinoculated with the empty plasmid, ZYMV or ZYMV-Ros1. Pictures were taken on 7 dpi. **B,** Groups of three *N. benthamiana* plants agroinoculated with the empty plasmid, ZYMV or ZYMV-Ros1 photographed at 21 dpi.

**SUPPLEMENTARY FIGURE S5**

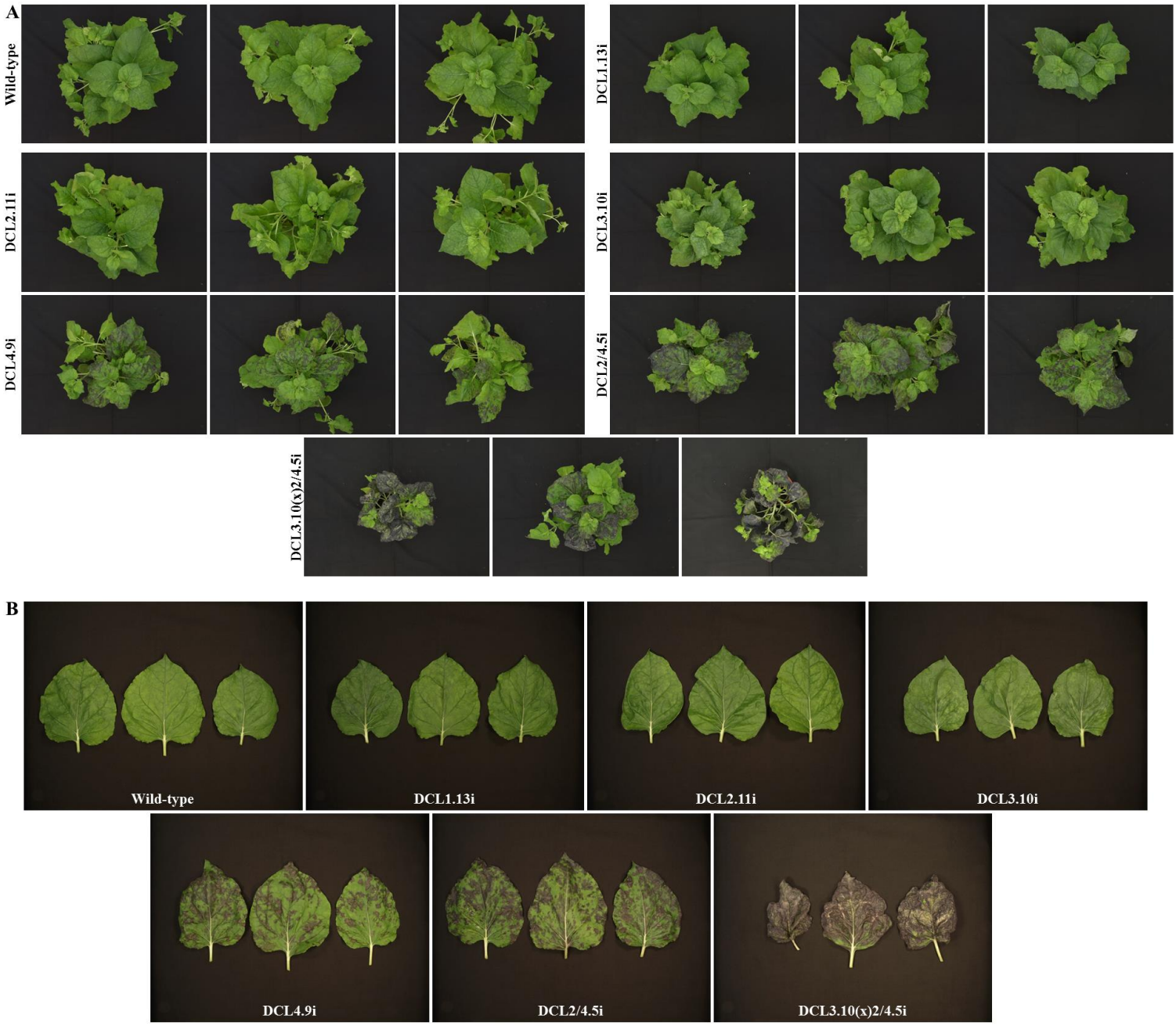


**Supplementary Fig. S5.** ZYMV-Ros1 more efficiently moves long-distance more efficiently in the *N. benthamiana* lines in which gene *DCL4* is down-regulated. **A,** Pictures taken at 27 dpi of the sets of the three *N. benthamiana* plants that correspond to wild-type and the *DCL* knock-down lines, as indicated, agroinoculated with ZYMV-Ros1. Close-ups of some of these pictures were used to create Fig. 4. **B,** Pictures taken at 27 dpi of selected leaves from the above plants to better appreciate the different patterns of anthocyanin accumulation.

## SUPPLEMENTARY FIGURE S6

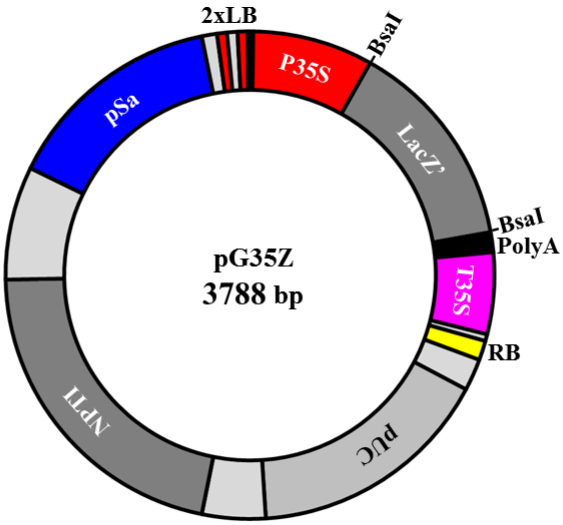


**>pG35z**

GCGGCCGC**GATTCCATTGCCCAGCTATCTGTCACTTTATTGTGAAGATAGTGGAAAAGGAAGGTGGCTCCTACAA**
**ATGCCATCATTGCGATAAAGGAAAGGCCATCGTTGAAGATGCCTCTGCCGACAGTGGTCCCAAAGATGGACCCCC**
**ACCCACGAGGAGCATCGTGGAAAAAGAAGACGTTCCAACCACGTCTTCAAAGCAAGTGGATTGATGTGATATCTC**
**CACTGACGTAAGGGATGACGCACAATCCCACTATCCTTCGCAAGACCCTTCCTCTATATAAGGAAGTTCATTTCA**
**TTTGGAGAGGGGAGACCATAAGCGG***CGCGTCCCATTCGCCATTCAGGCTGCGCAACTGTTGGGAAGGGCGATCGG*
*TGCGGGCCTCTTCGCTATTACGCCAGCTGGCGAAAGGGGGATGTGCTGCAAGGCGATTAAGTTGGGTAACGCCAG*
*GGTTTTCCCAGTCACGACGTTGTAAAACGACGGCCAGTGAGCGCGCGTAATACGACTCACTATAGGGCGAATTGG*
*AGCTCCACCGCGGTGGCGGCCGCTCTAGAACTAGTGGATCCCCCGGGCTGCAGGAATTCGATATCAAGCTTATCG*
*ATACCGTCGACCTCGAGGGGGGGCCCGGTACCCAGCTTTTGTTCCCTTTAGTGAGGGTTAATTGCGCGCTTGGCG*
*TAATCATGGTCATAGCTGTTTCCTGTGTGAAATTGTTATCCGCTCACAATTCCACACAACATACGAGCCGG**G**AGC*
*ATAAAGTGTAAAGCCTGGGGTGCCTAATGAGTGAGCTAACTCACATTAATTGCGTTGCGCTCACTGCCCGCTTTC*
**GGCGAATAGGTCTCG**AAAAAAAAAAAAAAAAAAAAAAAAAAAAAAAAAAAAAAAAAAAAAAAAAAAAAAAAAA**CGCTGAAATC**
**ACCAGTCTCTCTCTACAAATCTATCTCTCTCTATTTTCTCCATAAATAATGTGTGAGTAGTTTCCCGATAAGGGA**
**AATTAGGGTTCTTATAGGGTTTCGCTCATGTGTTGAGCATATAAGAAACCCTTAGTATGTATTTGTATTTGTAAA**
**ATACTTCTATCAATAAAATTTCTAATTCCTAAAACCAAAATCCAG**GGGCCCTCGACGTTCCT**TGACAGGATATAT**
**TGGCGGGTAAACTAAGTCGCTGTATGTGTTTGTTTG**AGATCCTCTAGGGCATGCAAGCTGATCTGGATCTCATGT
GAGCAAAAGGCCAGCAAAAGGCCAGGAACCGTAAAAAGGCCGCGTTGCTGGCGTTTTTCCATAGGCTCCGCCCCC
CTGACGAGCATCACAAAAATCGACGCTCAAGTCAGAGGTGGCGAAACCCGACAGGACTATAAAGATACCAGGCGT
TTCCCCCTGGAAGCTCCCTCGTGCGCTCTCCTGTTCCGACCCTGCCGCTTACCGGATACCTGTCCGCCTTTCTCC
CTTCGGGAAGCGTGGCGCTTTCTCATAGCTCACGCTGTAGGTATCTCAGTTCGGTGTAGGTCGTTCGCTCCAAGC
TGGGCTGTGTGCACGAACCCCCCGTTCAGCCCGACCGCTGCGCCTTATCCGGTAACTATCGTCTTGAGTCCAACC
CGGTAAGACACGACTTATCGCCACTGGCAGCAGCCACTGGTAACAGGATTAGCAGAGCGAGGTATGTAGGCGGTG
CTACAGAGTTCTTGAAGTGGTGGCCTAACTACGGCTACACTAGAAGAACAGTATTTGGTATCTGCGCTCTGCTGA
AGCCAGTTACCTTCGGAAGAAGAGTTGGTAGCTCTTGATCCGGCAAACAAACCACCGCTGGTAGCGGTGGTTTTT
TTGTTTGCAAGCAGCAGATTACGCGCAGAAAAAAAGGATCTCAAGAAGATCCTTTGATCTTTTCTACGGGGTCTG
ACGCTCAGTGGAACGAAAACTCACGTTAAGGGATTTTGGTCATGAGATTATCAAAAAGGATCTTCACCTAGATCC
TTTTAAATTAAAAATGAAGTTTTAAATCAATCTAAAGTATATATGTGTAACATTGGTCTAGTGATTAGAAAAACT
CATCGAGCATCAAATGAAACTGCAATTTATTCATATCAGGATTATCAATACCATATTTTTGAAAAAGCCGTTTCT
GTAATGAAGGAGAAAACTCACCGAGGCAGTTCCATAGGATGGCAAGATCCTGGTATCGGTCTGCGATTCCGACTC
GTCCAACATCAATACAACCTATTAATTTCCCCTCGTCAAAAATAAGGTTATCAAGTGAGAAATCACCATGAGTGA
CGACTGAATCCGGTGAGAATGGCAAAAGTTTATGCATTTCTTTCCAGACTTGTTCAACAGGCCAGCCATTACGCT
CGTCATCAAAATCACTCGCATCAACCAAACCGTTATTCATTCGTGATTGCGCCTGAGCAAGACGAAATACGCGAT
CGCTGTTAAAAGGACAATTACAAACAGGAATCGAATGCAACCGGCGCAGGAACACTGCCAGCGCATCAACAATAT
TTTCACCTGAATCAGGATATTCTTCTAATACCTGGAATGCTGTTTTCCCTGGGATCGCAGTGGTGAGTAACCATG
CATCATCAGGAGTACGGATAAAATGCTTGATGGTCGGAAGAGGCATAAATTCCGTCAGCCAGTTTAGTCTGACCA
TCTCATCTGTAACAACATTGGCAACGCTACCTTTGCCATGTTTCAGAAACAACTCTGGCGCATCGGGCTTCCCAT
ACAATCGGTAGATTGTCGCACCTGATTGCCCGACATTATCGCGAGCCCATTTATACCCATATAAATCAGCATCCA
TGTTGGAATTTAATCGCGGCCTTGAGCAAGACGTTTCCCGTTGAATATGGCTCATAACACCCCTTGTATTACTGT

TTATGTAAGCAGACAGTTTTATTGTTCATGATGATATATTTTTATCTTGTGCAATGTAACATCAGAGATTTTGAG
ACACAACGTGGCTTTGTTGAATAAATCGAACTTTTGCTGAGTTGAAGGATCAGATCACGCATCTTCCCGACAACG
CAGACCGTTCCGTGGCAAAGCAAAAGTTCAAAATCACCAACTGGTCCACCTACAACAAAGCTCTCATCAACCGTG
GCTCCCTCACTTTCTGGCTGGATGATGGGGCGATTCAGGCGATCCCCATCCAACAGCCCGCCGTCGAGCGGGCTT
TTTTATCCCCGGAAGCCTGTGGATAGAGGGTAGTTATCCACGTGAAACCGCTAATGCCCCGCAAAGCCTTGATTC
ACGGGGCTTTCCGGCCCGCTCCAAAAACTATCCACGTGAAATCGCTAATCAGGGTACGTGAAATCGCTAATCGGA
GTACGTGAAATCGCTAATAAGGTCACGTGAAATCGCTAATCAAAAAGGCACGTGAGAACGCTAATAGCCCTTTCA
GATCAACAGCTTGCAAACACCCCTCGCTCCGGCAAGTAGTTACAGCAAGTAGTATGTTCAATTAGCTTTTCAATT
ATGAATATATATATCAATTATTGGTCGCCCTTGGCTTGTGGACAATGCGCTACGCGCACCGGCTCCGCCCGTGGA
CAACCGCAAGCGGTTGCCCACCGTCGAGCGCCTTTGCCCACAACCCGGCGGCCGGCCGCAACAGATCGTTTTATA
AATTTTTTTTTTTGAAAAAGAAAAAGCCCGAAAGGCGGCAACCTCTCGGGCTTCTGGATTTCCGATCCCCGGAAT
TAGATCCGTTTAAACTACGTAAGATCGATCT**TGGCAGGATATATTGTGGTGTAAAC**GTTCCTGCGGCGGTCGAGA
TGGATCT**TGGCAGGATATATTGTGGTGTAAAC**GTTCCT

**Supplementary Fig. S6.** Map and sequence of binary vector pG35Z. The plasmid contains a cloning site that consists in two inverted BsaI cleavage sites separated by a Lac*Z*' (β-galactosidase α peptide from *E. coli*) selection marker. The two BsaI recognition sites are on a green background with the corresponding cleavage sites underlined. The LacZ' cassette is in italics. The CaMV 35S promoter (P35S in the map) is in red with the +1 nucleotide on a yellow background. The CaMV 35S transcription terminator (T35S in the map) is in fuchsia with the polyadenylation site underlined. The T-DNA right border (RB in the map) is on a yellow background with the overdrive sequence underlined. The pUC replication origin for *E. coli* is on a gray background. Kanamycin resistance marker (NPTI in the map) is on a dark gray background. This marker contains a silent mutation (in red) to eliminate an undesired BsmBI restriction site. The pSa replication origin for *A. tumefaciens* is in blue on a gray background. A double T-DNA left border (2×LB in the map) is on a red background.